Pergamon

Geochimica et Cosmochimica Acta, Vol. 61, No. 20, pp. 4297–4307, 1997

0016-7037/97 $17.00 + .00

PII S0016-7037(97)00211-1

# Short-time dissolution mechanisms of kaolinitic tropical soils

NATHALIE MALENGREAU and GARRISON SPOSITO
Division of Ecosystem Sciences, Hilgard Hall, MC3110, University of California, Berkeley, California 94720-3110, USA

(*Received April* 3, 1996; *accepted in revised form June* 5, 1997)

**Abstract**—Previous research on the short-time dissolution behavior of kaolinitic Oxisols suggested pH-dependent kinetics involving ligand-promoted dissolution, metal readsorption, and colloidal dispersion, with soil organic matter conjectured to play a decisive role. A novel combination of spectroscopy, light-scattering, and batch dissolution experiments, conducted at controlled pH and ionic strength over five dissolution periods ranging from 1 to 12 h, was applied to evaluate this mechanism for samples of a representative kaolinitic Oxisol collected at both forested and cultivated field sites (leading to significant differences in organic matter content and field soil pH). The overall characteristics of the pH-dependent net release kinetics of Al, Fe, and Si by the soil samples, for any dissolution period in the range investigated, were determined by the pH value at which colloid dispersion commenced, which decreased significantly as the soil organic matter content increased. Plots of log(Si/Al released) (or Si/Fe released) vs. $-\log [H^+]$ ($[H^+]$ is proton concentration) were superimposable for all dissolution periods studied, rising to a plateau value above the point of zero net charge of the soils (pH 3.2). Light-scattering and X-ray diffraction data showed conclusively that this plateau represented the release of siliceous colloids containing kaolinite and X-ray amorphous material. X-ray diffraction, UV-visible diffuse reflectance spectroscopy, and electron spin resonance spectroscopy, applied to the soil samples before and after dissolution, and after conventional chemical extractions to remove Al, C, Fe, and Si, showed that kaolinite and iron oxide phases (the latter being highly Al-substituted and present in both coatings and occlusions) were essentially unaltered by dissolution, even at $-\log [H^+] = 2$, whereas substantial dissolution loss of soil quartz occurred. Diffuse reflectance spectroscopy gave strong evidence that C in these soils occurs principally in discrete solid phases, not as a reactive coating on mineral surfaces. *Copyright © 1997 Elsevier Science Ltd*

## 1. INTRODUCTION

Nonspodic forested soils in the humid tropics comprise solid-phase mixtures of quartz, secondary kaolinite accompanied by small amounts of aluminum and iron oxides with trace amounts of hydroxy-vermiculite, and humified organic matter (Herbillon, 1980). The secondary soil minerals can differ substantially from their geologic counterparts in respect to composition, particle size, and reactivity toward dissolved solutes (Schwertmann and Herbillon, 1992; Singh and Gilkes, 1993). Adding to the complexity of these soil solid phases is their potential to retain oxide, clay mineral, and organic matter as either coatings or occlusions that develop from precipitated products of biogeochemical weathering (Mulder and Stein, 1994; Michalopoulos and Aller, 1995).

Chorover and Sposito (1995b) recently measured the three-hour release kinetics of Al, Fe, Si, and C from four representative kaolinitic tropical soils (Oxisols) during batch dissolution experiments that were conducted at controlled pH and ionic strength (LiCl background electrolyte). The net release of Al and Fe from a soil, plotted as a function of pH, exhibited a distinct point of minimum dissolution (p.m.d.), at which metal release was least over the pH range, 2–7. The values of the p.m.d. were somewhat above the point of zero net charge (p.z.n.c.) of the soils. The net release of C and Si by the soils showed a much weaker pH dependence, although the molar ratio of Si to Al released (and of Si to Fe released) grew to achieve a plateau above the p.m.d., in part because of released Al and Fe readsorption as pH was increased (Chorover and Sposito, 1995b). Finding that oxalate-extractable Al in the soils was approximately equal to the maximum Al released after 3 h dissolution, Chorover and Sposito (1995b) conjectured that organic matter played an important role in the soil dissolution process. Above the p.m.d., Al, Fe, and Si were released in colloidal particulate forms. Colloids extracted from the soils were investigated in greater detail by Chorover and Sposito (1995c), who found that they dispersed readily at pH ≥ p.z.n.c. and exhibited very low isoelectric points (i.e.p.) ≤2.5, well below those typical of aluminum or iron oxide minerals (Sposito, 1992). These and other experimental results led Chorover and Sposito (1995c) to suggest that organic matter coatings on the colloids might have a significant role in their dispersive behavior.

The study of Chorover and Sposito (1995b), although illuminating, was conducted only for a single, fixed dissolution period of 3 h, which was selected primarily because it was longer than the time required for the equilibration of pH (<20 min), while being short enough to avoid reaching steady-state dissolution conditions (Chorover and Sposito, 1995a). Whether a p.m.d. would exist for short-time dissolution periods less than or longer than 3 h is unknown, and no direct information is available about the exact disposition of organic matter or its effects on dissolution of the minerals in the Oxisols they investigated. In the present paper we extend the experiments of Chorover and Sposito (1995b) to include 1, 3, 6, 9, and 12 h of dissolution at controlled pH and ionic strength, and we apply light-scattering methods, X-ray diffraction, UV-visible diffuse reflectance spectros-

copy, and electron spin resonance spectroscopy to ascertain the fate of mineral and organic matter phases as dissolution proceeded. The principal objectives of our study were to elucidate the origin of the p.m.d. and to examine the behavior of key solid-phase components in kaolinitic Oxisols during short-time dissolution.

Chorover and Sposito (1995b) found that net Al and Fe release from the four Oxisols they investigated was not sensitive to the content of crystalline aluminum and iron oxides or kaolinite. Therefore, just one of their representative soils (Manaus series) was used in the present study. On the other hand, they did infer that plant canopy differences (forest cover vs. row crops in annual rotation) impacted both the dissolution characteristics and the colloidal chemistry of the soils (Chorover and Sposito, 1995b,c). Therefore, two different samples of the Manaus soil, collected in proximate forested or cultivated field plots, were used in our experiments.

## 2. EXPERIMENTAL METHODS

### 2.1. Soil Samples

Samples of the surface horizon of a kaolinitic soil, collected at an EMBRAPA experiment station 30 km outside Manaus (Amazonas State, Brazil), were provided in 1991 by Dr. Cheryl Palm (Natural Resource Ecology Laboratory, Colorado State University). The soil is classified in the U.S. Soil Taxonomy as a Xanthic Hapludox (Oxisol order). Details of the field sampling procedures and overall characterization of the soil are given by Motavalli et al. (1994, 1995). One sample (MF1) was obtained at a moist tropical rainforest site, whereas the other (MC) was obtained from a nearby experimental site that had been under continuous cultivation since 1982 (annual corn-cowpea rotation). The soil samples were stored moist at 4°C prior to use in the dissolution experiments.

Physical and chemical properties of the two soil samples have been described in detail by Chorover and Sposito (1995b). Both samples contain 75 wt% clay and both have a point of zero net charge (p.z.n.c.) at 3.2. Sample MC differs from sample MF1 by containing less C (1.7 vs. 3.3 wt%) and having a higher saturated-paste pH value (5.3 vs. 4.2). These differences are typical of cultivated vs. uncultivated acidic soils.

### 2.2. Dissolution Experiments

#### 2.2.1. Batch experiments

Batch dissolution studies of the two soil samples suspended in 0.005 mol $kg^{-1}$ LiCl at 22 ± 2°C were conducted following the procedure of Chorover and Sposito (1995b). Briefly, each soil sample was prepared in homoionic form, by reaction with LiCl solution, to remove exchangeable lithogenic cations, including $Al^{3+}$ that would be a complicating source of rapidly-mobilized Al (Chorover and Sposito, 1995b). Mixed solutions of LiCl/HCl/LiOH were combined with the homoionic soil paste to yield a suspension with a solids concentration of 10 g $kg^{-1}$ and $-\log [H^+]$ values between 2 and 6. Equilibration of the proton concentration was always rapid (variation $\leq 0.2$ in $\log [H^+]$ after equilibrating 0.3 h) on the timescale of the dissolution experiments, as noted also by Chorover and Sposito (1995b). Therefore, constant values of $-\log [H^+]$ were sustained for essentially 12 h in the dissolution experiments. At initial $-\log [H^+] < 4$, equilibration produced no detectable change in proton concentration, whereas at initial $-\log [H^+] > 4$, there was an immediate shift toward equilibration near $-\log [H^+] = 5.5$. The suspensions were rotated gently for 1, 3, 6, 9, or 12 h, then centrifuged at 27,000 RCF for 20 min to separate the supernatant solution. This aqueous phase was subsampled immediately to measure $-\log [H^+]$, the remainder then being acidified to pH 2 with $HNO_3$ and stored at 4°C prior to chemical analysis. The residual soil paste also was stored at 4°C in sealed centrifuge tubes.

#### 2.2.2. Chemical analyses

Concentrations of Al, Ca, Fe, Mg, and Si in the supernatant solution were measured by inductively-coupled plasma atomic emission spectroscopy (ICPAES) using a Perkin-Elmer Plasma 40 spectrometer. Calibration solutions were prepared on a mass basis using ICPAES reference standards. The LiCl solution used in the dissolution experiments was also analyzed. The concentration of dissolved organic carbon (DOC) in the supernatant solutions was measured by UV-promoted persulfate oxidation followed by infrared detection with a Dohrmann DC-80 carbon analyzer. Proton concentrations in the supernatant solutions were measured with an Orion-Ross combination electrode calibrated by Gran titration as described by Chorover and Sposito (1995a). After LiCl saturation, triplicate 500 mg subsamples of soil paste were transferred to acid-washed, oven-dried ceramic crucibles. The pastes were dried to constant mass at 110°C to determine water content. Millimoles of Al, C, Ca, Fe, Mg, and Si released per kilogram of dry soil were then calculated.

#### 2.2.3. Light-scattering experiments

Light scattered by the acidified supernatant solutions that were separated after the dissolution experiments was measured in quartz cells using a Perkin-Elmer MPF-66 luminescence spectrophotometer with excitation and emission wavelengths fixed at 643 nm. Successive readings of time-integrated (20 s) scattering intensities were taken. Light scattered by 0.005 mol $kg^{-1}$ LiCl solution as used in the dissolution experiments was measured in the same way, its intensity then being subtracted from that of the supernatant solution to determine the colloidal light scattering intensity. The supernatant solutions separated after 9 h dissolution at $-\log [H^+] = 5$ (sample MC) or 6 (sample MF1) were freeze-dried and saved for mineralogical analysis of the solid residue.

#### 2.2.4. Mineralogical analyses

X-ray diffraction (XRD) was used to identify crystalline minerals in unfractionated soil samples, both before and after the dissolution experiments, as well as in the residual solid material recovered from the supernatant solutions by freeze-drying them after separation. Powder diffractograms were recorded with a PW 1710 vertical goniometer (40 KV, 30 mA) using CoK$\alpha$ radiation ($\lambda_{Co}$ = 1.7902 Å). Data were collected in the step-scanning mode, counting radiation for 15 s in 0.03 °2$\theta$ increments between 3 and 120 °2$\theta$ for the soils, and for every 20 s in 0.04 °2$\theta$ increments between 3 and 70° 2$\theta$ for the colloidal particles. One-degree (1°) divergence and antiscattering slits and a 0.2 mm receiving slit were used. Peak positions were calibrated with a Si plate. The soil samples were backmounted in Al holders by packing them against cardboard to obtain a flat surface while minimizing preferential particle orientation. The colloidal particle samples obtained by freeze-drying of the supernatant solutions did not have sufficient mass to permit backmounting. Instead, they were allowed to settle in ethanol on a Si plate wrapped with Al foil.

X-ray diffraction lineshapes for the soil samples prior to dissolution were computed with the Rietveld refinement procedure, which uses a model to approximate an actual crystal structure. This procedure does not require determination of individual Bragg intensities, since each data point in the diffractogram is used as an observation in the structure refinement. Parameters were varied (least-squares method) until the differences between observed and calculated diffraction patterns were minimized (Post and Bish, 1988; Bish and Von Dreele, 1989). Quantitative analysis of the diffraction data was performed using the XND code (Bérar, 1990, cited by Morin, 1994) to obtain estimates of the percentages of component crystalline phases in the soils. The Voigt function was used to fit the individual reflection profiles.

### 2.3. Spectroscopic Measurements

#### 2.3.1. Diffuse reflectance spectroscopy (DRS)

The two soil samples were examined by DRS over the wavelength range 200–800 nm both prior to and after the dissolution experiments, as well as after conventional chemical extractions that re-

moved Al, C, Fe, and Si (see Table 2). Extraction with either aqueous 1:1 methanol solution or aqueous 1:10 $H_2O_2$ solution was used to remove organic matter by stirring in suspension for 1 h at laboratory temperature. Sodium dithionite-citrate-bicarbonate extraction (DCB; (Mehra and Jackson, 1960) was combined with the dithionite-Tamm (ammonium oxalate + oxalic acid) extraction as adapted by Hétier and Jeanroy (1973). Samples were shaken end-by-end in a waterbath at 80°C for 1 h in each extraction. This combined extraction is purported to remove Fe in oxides irrespective of their crystalline order. The ammonium oxalate extraction of Tamm (1922) is considered to remove Al, Fe, and Si in poorly-ordered inorganic as well as in organic chemical forms. Samples were shaken 4 h at laboratory temperature with exclusion of light. Extraction with sodium pyrophosphate (Farmer et al., 1983) was performed to remove Al and Fe in organic chemical forms. Samples were shaken 16 h at laboratory temperature. Selected samples of the two soils taken after the dissolution experiments also were studied by DRS.

Diffuse reflectance spectra in the UV-visible range were obtained in digital form using a Cary 2300 spectrophotometer. Measurements were referenced to a Halon standard (Weidner and Hsia, 1981) and fit to cubic spline functions to reduce spectral noise (Reinsch, 1967). Soils are usually neither completely transparent nor completely opaque to incident visible light, i.e., soil particles partly absorb and partly scatter the light. The Kubelka-Munk (KM) formalism takes into consideration light scattering as well as absorption processes to provide information about the nature of these particles (Wendlandt and Hecht, 1996; Barron and Torrent, 1986). A remission function $F(R)$ is defined by

$$F(R) = \frac{(1 - R)^2}{2R} = \frac{K}{S}$$

in which $R$ is the diffuse reflectance of a sample, and $K$ and $S$ are the absorption and scattering coefficients, respectively (Wendlandt and Hecht, 1996). The scattering coefficient $S$ depends on particle size, as well as on particle shape and packing. The absorption coefficient $K$ depends on the nature of the absorbers in the scattering solid phases. The use of the KM formalism thus gives a general synopsis of the effects of soil texture and mineralogy on optical spectra. Remission functions obtained in the present study were normalized by the intensity of the OH overtone of kaolinite near 1400 nm.

A typical diffuse reflectance spectrum of natural particulate materials results from the superposition of absorption bands on a rising spectral slope that is related to particle shape, size, or orientation. Poorly-defined absorption bands can be located and poorly-resolved bands can be separated more precisely by examining the second derivative of the spectrum (Cahill, 1979; Huguenin and Jones, 1986; Malengreau et al., 1994, 1997). In the present study, this technique was used to detect iron oxides in the two soil samples and to monitor their status after the dissolution experiments. A detailed description of this type of application for second-derivative DRS is given by Malengreau et al. (1996). Band positions were determined from minima in second-derivative curves to within ±3–4 nm, as estimated by Malengreau et al. (1994) considering spectrometer resolution and the errors caused by numerical smoothing and calculation of derivatives.

#### 2.3.2. *Electron spin resonance (ESR) spectroscopy*

Air-dried powder samples of the two soils, prepared before and after dissolution, were packed into quartz ESR tubes to a uniform height of 15 mm, following which spectra were recorded at X-band (ca. 9.74 GHz) and Q-band (ca. 34 GHz) frequencies on a Bruker ESP 300E spectrometer. The higher-frequency Q-band gives greater sensitivity and increases the separation between electron spin energy levels, allowing the acquisition of better-resolved spectra. The fixed experimental parameters were: 100 kHz modulation frequency, 50 mW microwave power, 5 G or 15 G amplitude for the modulation field, and a time constant ranging from 0.163 to 0.327. The ESR spectra were recorded at room temperature. Spectroscopic $g$-values were calibrated by comparison with a 1,1-diphenyl-2-picryl hydrazyl (DPPH) standard ($g_{DPPH}$ = 2.0036).

## 3. RESULTS

### 3.1. Point of Minimum Dissolution

The time-trends of net Al, Fe, and Si release from both soil samples during dissolution (data not shown) were similar, showing a gradual rise in moles released with increasing dissolution time if $-\log [H^+] < 4$, but a general decline if $-\log [H^+] > 4$. The time-trends of net C, Ca, and Mg release (data not shown) were quite different from those of Al, Fe, and Si, exhibiting a broad maximum near 6 h (C) or 3 h (Ca and Mg), irrespective of the value of $-\log [H^+]$.

Graphs of the net moles of Al, C, and Si released from the two soil samples as a function of $-\log [H^+]$ at fixed equilibration time are shown in Figs. 1–3. For Al release, a point of minimum dissolution (p.m.d.) was observed near $-\log [H^+] = 3$ for sample MF1 only for equilibration times <6 h, whereas for soil sample MC, a p.m.d. near $-\log [H^+] = 4$ was quite discernible at all equilibration times investigated. After 6 h equilibration, sample MF1 showed only a monotonic decline in net Al release with increasing $-\log [H^+]$ (Fig. 1). Significant scatter in the analytical release data was apparent at $-\log [H^+] > 4$, suggesting the presence of particulate matter (note error bars in Fig. 1). The same pattern was exhibited by Fe release (data not shown). Release data for Si (Fig. 2) showed a weak minimum at $-\log [H^+] \approx 3$–4 for both soil samples, again with much scatter in the data at $-\log [H^+] > 4$. Organic C net release (Fig. 3) also showed a broad, weak minimum near $-\log [H^+] \approx 3$–4 for both soil samples at all equilibration times, but without the large increase in data scatter noted for Al, Fe, and Si.

Light scattering at 643 nm by the supernatant solutions separated from the soil suspension increased dramatically for $-\log [H^+] > 4$, especially for sample MF1, at any equilibration time up to 12 h (data not shown), confirming the more limited observations of Chorover and Sposito (1995b, Fig. 8). It is evident that colloidal particles retained in the supernatant solutions, even after centrifugation at 27,000 RCF, contributed to the elemental concentrations measured by ICPAES analysis. Plots similar in trend to Fig. 9 in Chorover and Sposito (1995b) were obtained by substituting the logarithm of Al, Fe, or Si concentration for that of $H^+$ as independent variable at equilibration time <12 h (data not shown), whereas no particular trend with DOC was discernible.

X-ray diffractograms of the freeze-dried colloidal particles in the supernatant solutions (Fig. 4) showed only a few sharp peaks, most of which correspond to reflections from kaolinite (Bailey, 1980), superimposed on a noisy, curvilinear background. Peaks at 2.03 and 3.68 Å are from Al foil used in the sample holder. The broad band centered around 3.6–3.8 Å is similar to that which is observed both for amorphous silica (Kastner, 1979; Singh and Gilkes, 1993) and for soil humic substances (Stevenson, 1994). This broad band is much more prominent in sample MF1 than in MC.

### 3.2. Solid-Phase Transformations

X-ray diffractograms for the unfractionated soil samples are shown in Fig. 5. Each is dominated by peaks attributable

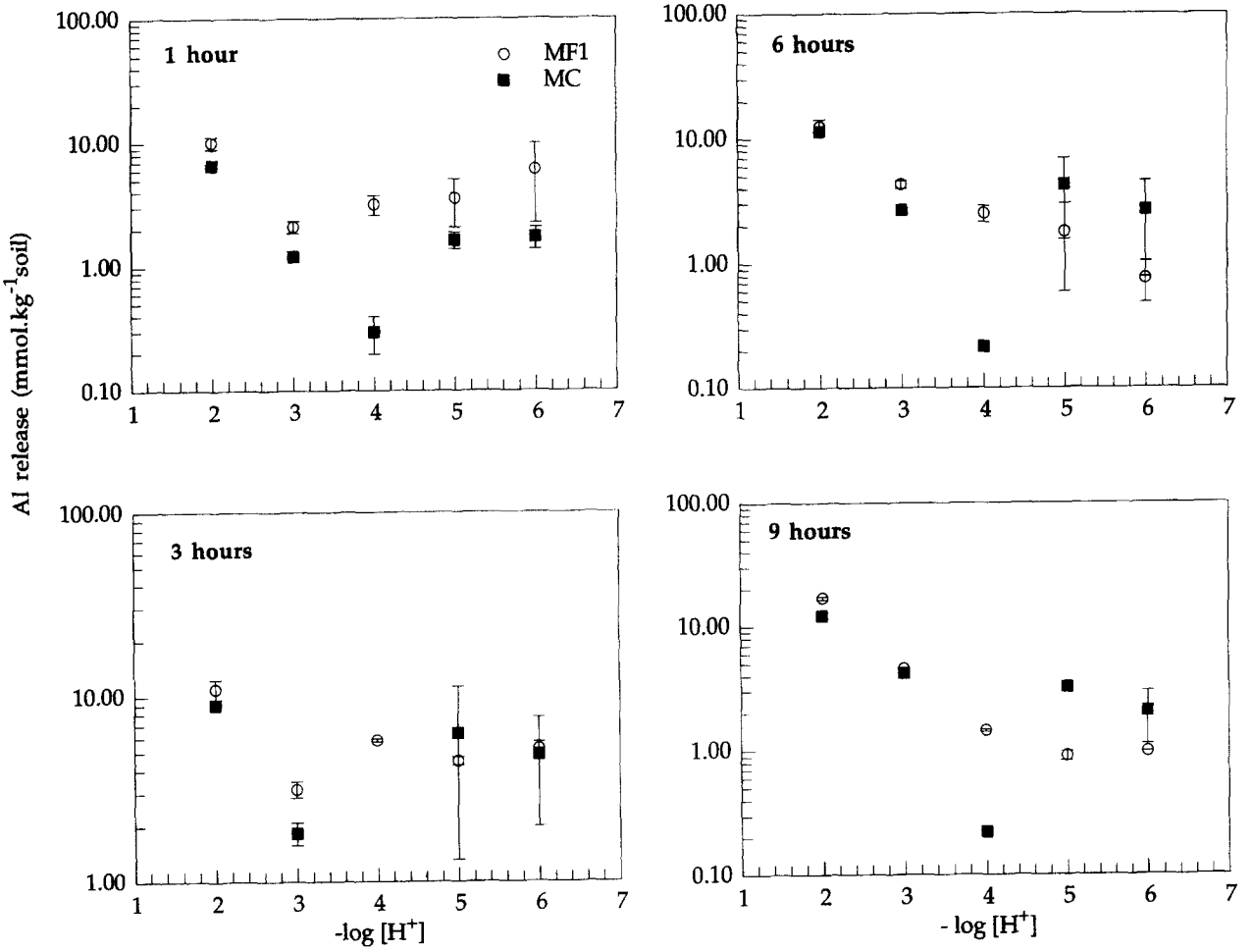


Fig. 1. Aluminum release from soils MF1 and MC in 0.005 mol $kg^{-1}$ LiCl solution as a function of initial $-\log [H^+]$, with dissolution period as a fixed parameter.

to kaolinite (K) and quartz (Q) (Table 1). The minor crystalline phases present are gibbsite (Gi), goethite (Go), anatase (An), and rutile (Ru). Structural disorder is apparent in the diffractograms, particularly in the 02l, 11l reflections (22–26° $2\theta$ CoK$\alpha$) and in the two sets of 13l, 20l reflections (40–46° $2\theta$ CoK$\alpha$), the degree of disorder being reminiscent of that observed commonly in tropical soil kaolinites (Herbillon, 1980; Santos et al., 1989; Schwertmann and Herbillon, 1992). The abundance of kaolinite makes quantification of the metal-oxide phases difficult, especially as to whether a poorly crystallized iron oxide is actually goethite or hematite. The major difficulty in quantifying these latter solid phases in association with kaolinite arises from the near congruence of the goethite and hematite 110 reflections (also the anatase 101 and rutile 110 reflections) with the most intense XRD peaks for kaolinite. The only clear diffraction line for iron oxides is observed at 2.69–2.70 Å; unfortunately, it is common both to goethite (130 reflection) and hematite (104 reflection). After dissolution for 12 h at $-\log [H^+] = 2$ (the longest reaction time and largest proton concentration investigated), none of the crystalline solid phases detected in the soil samples had disappeared (Fig. 5), and no change in the apparent degree of structural disorder of kaolinite was observed. However, a significant decrease in the intensity of the quartz peaks in the XRD pattern was seen. Calculations based on Rietveld refinement (Table 1) indicated that more than one-half of the quartz mass had been lost from the two soil samples.

Diffuse reflectance spectra of the two soils, without removal of organic matter, are presented in Fig. 6a. The spectra show broad absorption bands from electronic transitions in iron and titanium oxides, superimposed on a falling background (hereafter termed the continuum function) caused by light-scattering. The intense band observed at 300 nm can be attributed to $Fe^{3+}$-O charge-transfer transitions (Karickhoff and Bailey, 1973), while the sharp edge-feature occurring at about 370 nm is from Ti-O charge-transfer transitions. Its position, intermediate between that for rutile (403 nm) and that for anatase (359 nm), indicates that both primary and secondary titanium oxide minerals are present (Malengreau et al., 1995). Between 400 and 800 nm, the spectra display absorption bands caused by rearrangements of the electron configuration in d-orbitals of iron oxides (ca 430 and 495 nm for goethite and 525 nm for hematite). These bands are similar in both spectra, although the MF1 spectrum is shifted to higher values of the remission func-

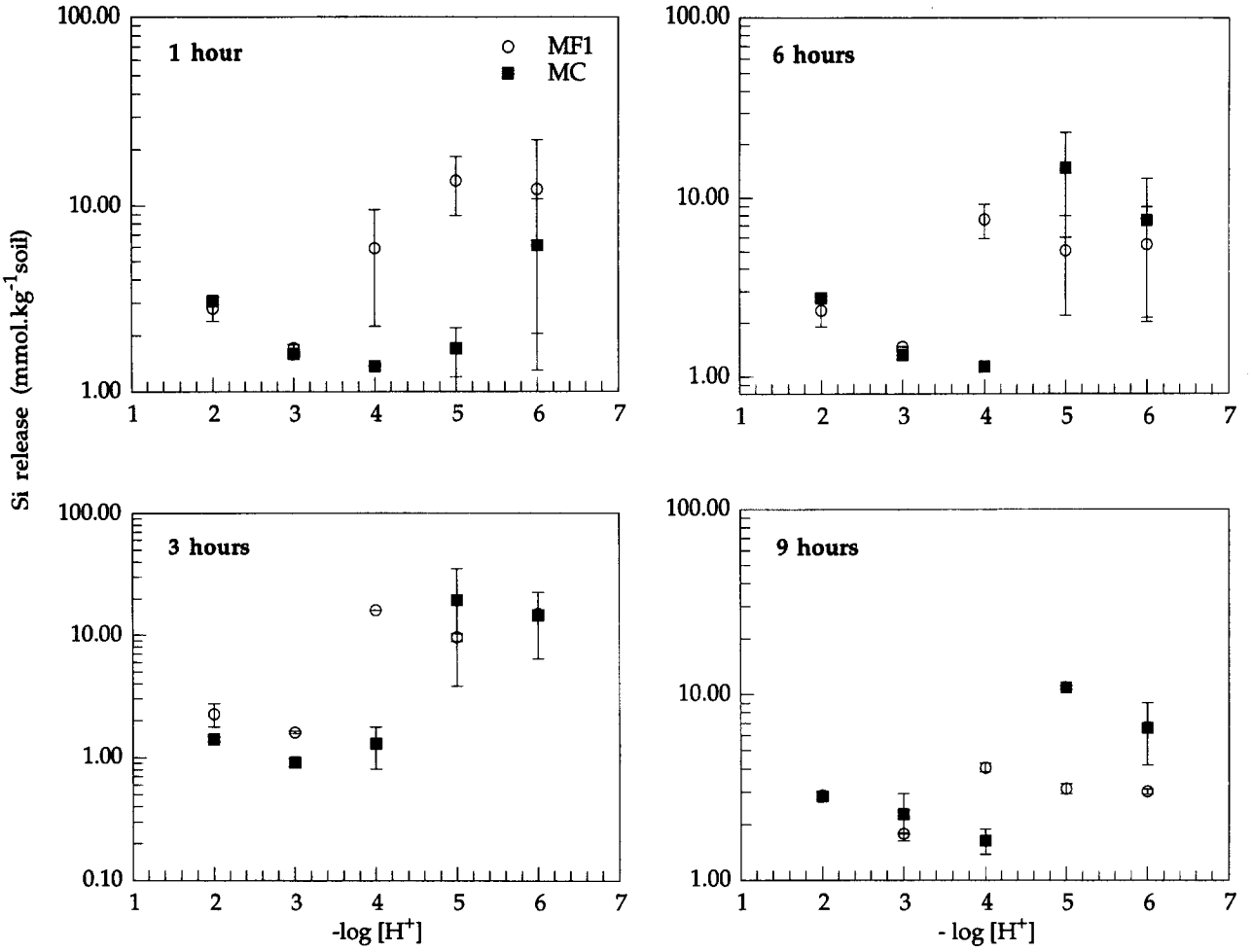


Fig. 2. Silicon release from soils MF1 and MC in 0.005 mol $kg^{-1}$ LiCl solution as a function of initial $-\log [H^+]$, with dissolution period as a fixed parameter.

tion, in agreement with the gray color of sample MF1 and pale ochre color of sample MC. The second-derivative spectra (Fig. 7) indicate two bands at about 420 and 474 nm that can be assigned to highly substituted Al-goethite, since this latter band is shifted to shorter wavelengths as compared to unsubstituted goethite (492 nm, Malengreau et al., 1994, 1997). A very weak band at about 525 nm indicates highly-substituted Al-hematite, but in very low quantity. High Al substitution of hematite and goethite, induced by low Si concentration and consequent high Al concentration when these iron oxides are formed (Schwertmann, 1985), leads to resistance to dissolution (Malengreau et al., 1996).

After DCB extraction, the absorption band for goethite shifted to that for unsubstituted goethite (496 nm) in both soils (Fig. 7). Malengreau et al. (1994) suggested that this can occur when iron oxide phases are occluded in kaolinite particles and the removal of iron oxide coatings permits spectroscopic detection of these occluded phases. The methanol, hydrogen peroxide, ammonium oxalate, and sodium pyrophosphate extractions resulted only in the entire diffuse reflectance spectrum being translated to lower values of the remission function, with the spectra of samples MF1 and MC then becoming almost superimposable (data not shown). This result indicates that only the gray level (as measured at 800 nm) became lower, but that the size-distribution, the texture of the scattering particles, and the iron oxide concentrations all were similar after these four extractions (Malengreau et al., 1994). This is strong evidence that organic matter occurs as a solid phase separate from the minerals in the soils. The spectral signature of organic matter coatings on the minerals would have been a broad absorption band ranging over the iron oxide spectrum in the visible range, such that this spectrum is obscured (Allard et al., 1992).

All of the post-dissolution spectra for both soils were similar to that shown for sample MC in Fig. 6b ($-\log [H^+] = 4$, 9h), with the exception of those for sample MF1 at pH 5 after 3 or 12 h reaction (data not shown) and for sample MC at $-\log [H^+] = 6$ after 3 h reaction (Fig. 6b). The principal result was a uniform shift in the remission function, showing that only the gray level was modified. Thus, no conclusion about changes in solid-phase reactivity is possible, but it can be stated that the size-distribution, form, and texture of the scattering particles were not altered by dissolution, because the remission function was only translated. For some spectra, this translation was not uni-

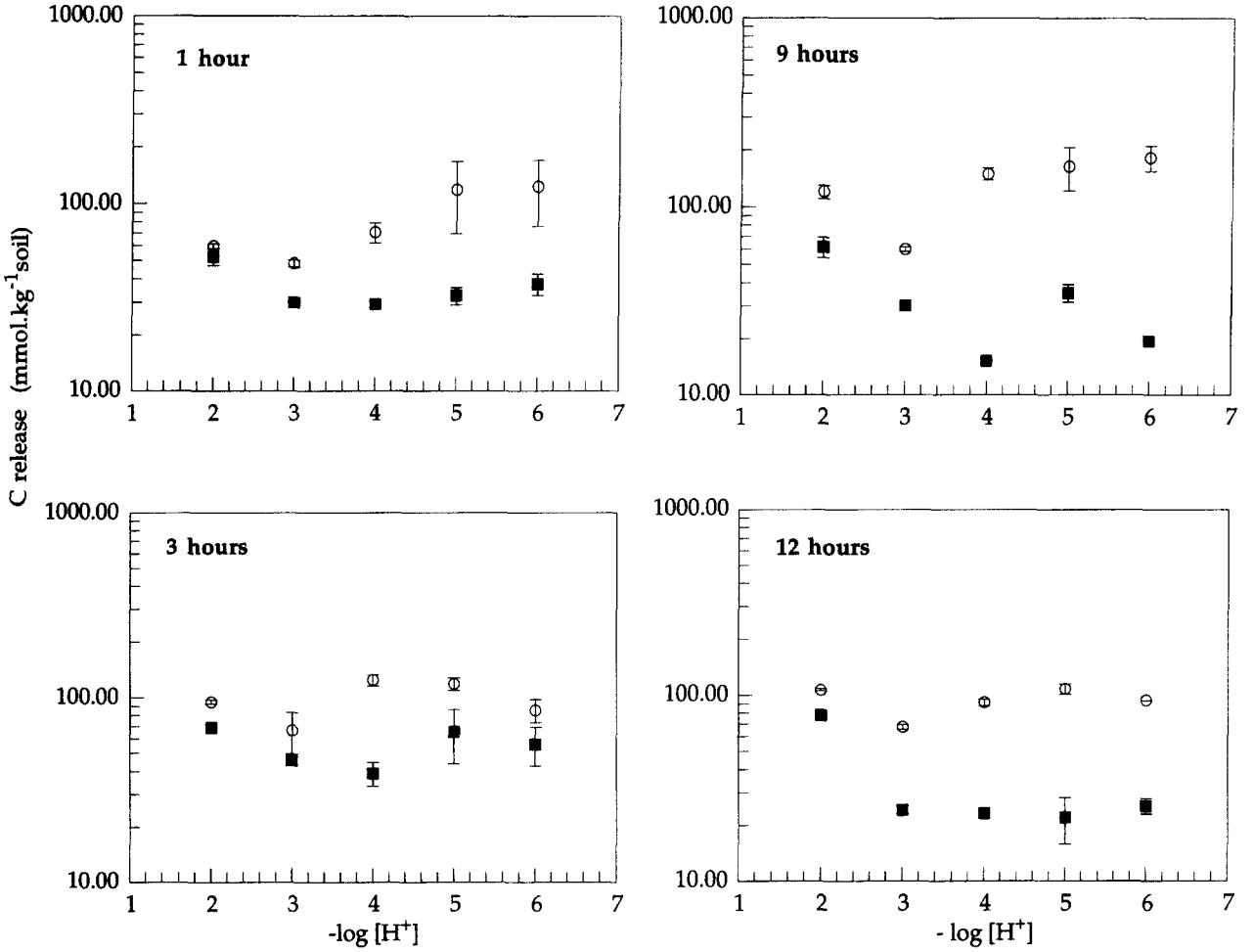


Fig. 3. Carbon release from soils MF1 and MC in 0.005 mol kg$^{-1}$ LiCl solution as a function of initial $-\log [H^+]$, with dissolution period as a fixed parameter.

form, showing a more important shift in the UV range. At $-\log [H^+] = 6$, in the cases noted above, the UV spectrum was flattened, while the 500–800 nm region remained unchanged or was translated toward different remission-function values (Fig. 6b). This wavelength-dependent behavior gave rise to spectral crossover that can be related to changes in particle form, size, and/or organization. In the present case, this is likely to have been caused by the selective loss of siliceous particles to the supernatant solution as a result of colloidal dispersion during dissolution. No spectral crossover was observed when light-scattering by the supernatant solution was nil.

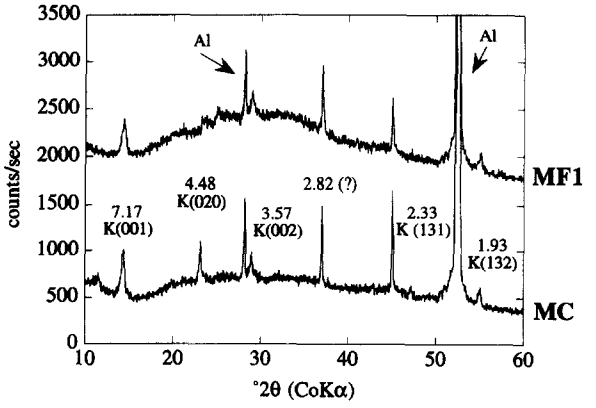


Fig. 4. XRD patterns for colloidal particles recovered from freeze-dried supernatant solutions after 9 h dissolution at $-\log [H^+] = 6$ (MF1) or 5 (MC). The strong Bragg reflections labeled Al are from an aluminum sample holder. The d-values (Å) and mineral phases are indicated above each peak: K = kaolinite.

The X- and Q-band ESR spectra of samples MF1 and MC were similar and remained unaffected by the dissolution reaction, even after 12 h equilibration at pH 2 (data not shown). The Q-band ESR spectra had better resolution, allowing clear discernment of hyperfine structure (Fig. 8). The signal at $g = 4$ in Fig. 8a is from $Fe^{3+}$ in two crystallographically distinct sites (Hall, 1980; Brindley et al., 1986): rhombically-distorted and those with a slight axial distortion. The signal observed at $g = 2$ represents a broad resonance from superparamagnetic iron oxides superimposed on a sharp signal from paramagnetic centers that are radiation-induced defects (RID) in kaolinite (Angel et al., 1974; Muller and Calas, 1993b; Clozel et al., 1994). Around 12,000 G, the ESR spectra show a sharp, intense feature

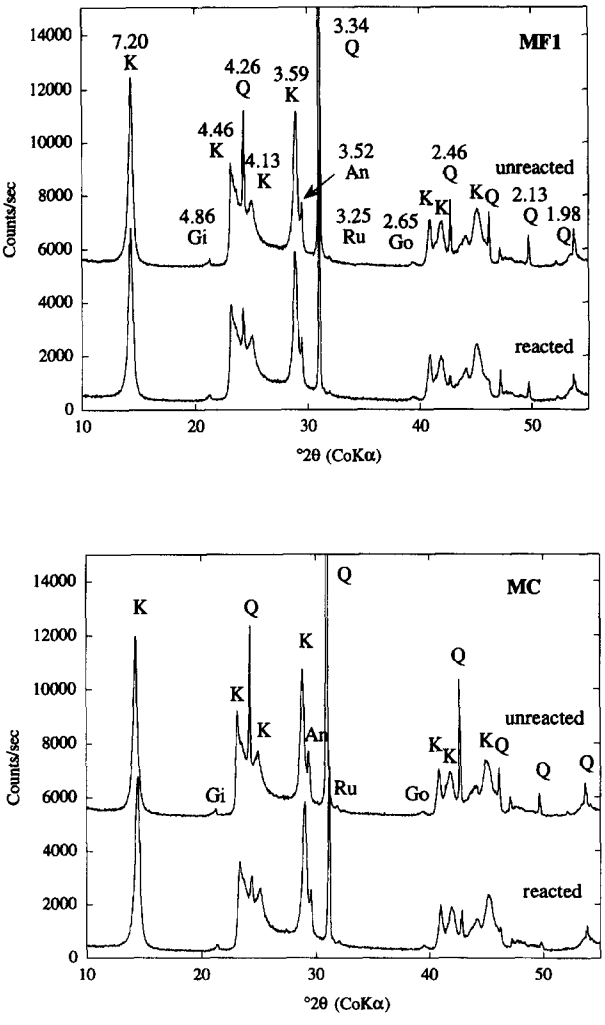


Fig. 5. XRD patterns for soils MF1 and MC before dissolution (unreacted) and after 12 h dissolution at $-\log [H^+] = 2$ (reacted). The $d$-values (Å) and mineral phases are indicated above each peak. K = kaolinite, Q = quartz, Gi = gibbsite, Go = goethite, An = anatase and Ru = rutile.

corresponding to RID. All of the other, nonlabeled features in Fig. 8a can be attributed to structural Fe (Meads and Malden, 1975; Hall, 1980). A broad signal centered on the 12,000 G region can be assigned to superparamagnetic iron oxides. Expanding the 11,000–13,000 G range (Fig. 8b),

Table 1. Mineralogical composition of soil samples MF1 and MC as determined by Rietveld refinement of X-ray diffractograms (relative error is about 10%).

| | (wt %) | | | | | |
|---|---|---|---|---|---|---|
| Soil | Kaolinite | Quartz | Gibbsite | Goethite | Anatase | Rutile |
| MF1 | 77 | 18 | 0.4 | 1.2 | 3.5 | 0.9 |
| MF1 diss[a] | 85 | 8.0 | 0.4 | 1.3 | 3.9 | 1.1 |
| MC | 76 | 19 | 0.4 | 0.6 | 3.6 | 1.0 |
| MC diss[a] | 87 | 6.4 | 5 | 0.7 | 4.4 | 1.1 |

[a] Soil sample reacted at pH 2 in 0.005 mol $kg^{-1}$ LiCl for 12 h.

Table 2. Aluminum, silicon, and iron extracted (dry soil mass basis) by three chemical treatments: Na dithionite-citrate-bicarbonate (DCB); $NH_4$ oxalate (TAMM); and Na pyrophosphate (PYRO). Mean deviations in parentheses.

| | (mmol $kg^{-1}$) | | |
|---|---|---|---|
| Extraction Soil | Al | Si | Fe |
| DCB | | | |
| MF1 | 143 (4) | 6 (0.4) | 42 (0) |
| MC | 169 (3) | 12 (0.1) | 44 (0) |
| TAMM | | | |
| MF1 | 59 (1) | 4 (0.7) | 34 (2) |
| MC | 42 (2) | 3 (0.2) | 22 (1) |
| PYRO | | | |
| MF1 | 77 (0) | 26 (0.4) | 39 (0) |
| MC | 90 (2) | 26 (0.3) | 44 (0) |

we noted an apparent six-line hyperfine structure superimposed on the RID feature in the MF1 spectrum, but very weak or absent in the MC spectrum. The linewidth ($\Delta B$) between two of the six-line components is 30 G. This pattern

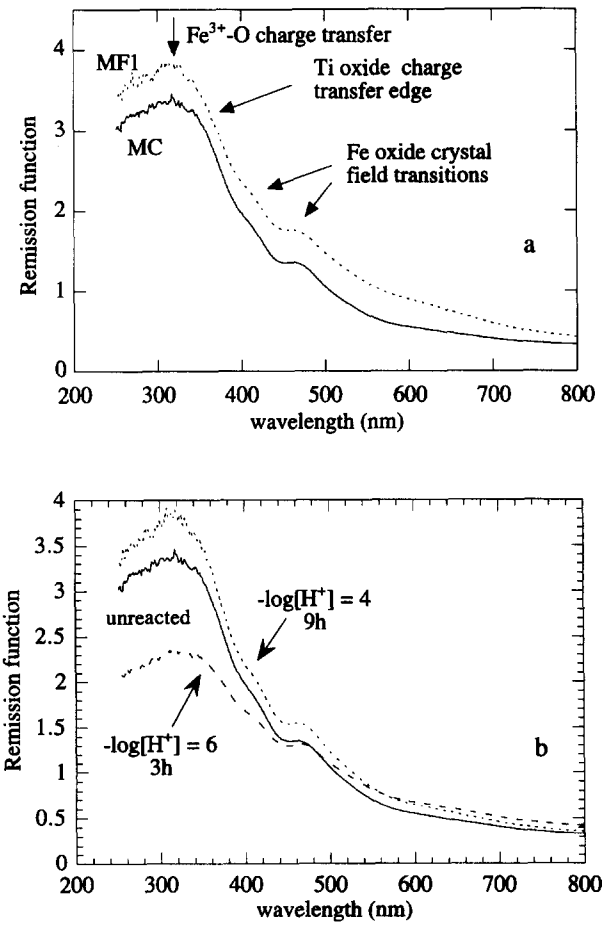


Fig. 6. (a) Diffuse reflectance spectra of soils MF1 and MC in the UV-visible range, normalized to the OH overtone feature of kaolinite (1400 nm). (b) Diffuse reflectance spectra of soil MC before (unreacted) and after 9 h dissolution at $-\log [H^+] = 4$, or 3 h dissolution at $-\log [H^+] = 6$.

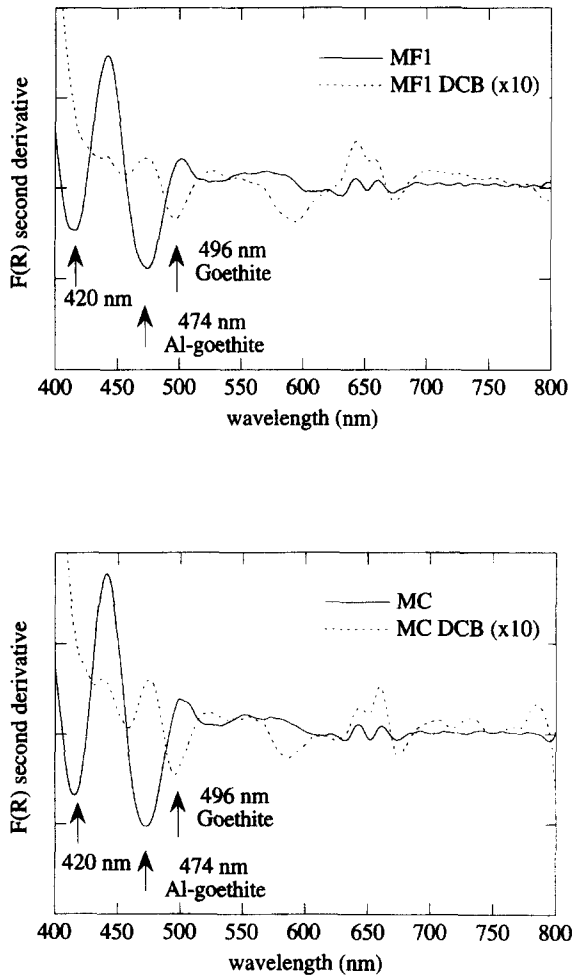


Fig. 7. Second-derivative diffuse reflectance spectra of soil MF1 and MC in the UV-visible range before (solid line) and after (dashed line) dithionite-citrate-bicarbonate treatment (DCB).

is indicative of $Mn^{2+}$ (Meads and Malden, 1975; Hall, 1980).

## 4. DISCUSSION

### 4.1. Origin of the p.m.d.

Perhaps the most striking difference between our dissolution data and those of Chorover and Sposito (1995b) is the disappearance of a p.m.d. for Al release by sample MF1 after 3 h equilibration, whereas sample MC exhibited a p.m.d. at all equilibration times investigated (Fig. 1). Despite this important difference, the trend in log (Si/Al) released vs. $-\log [H^+]$ (Fig. 9) was very similar at all equilibration times, and for both soil samples, showing a gradual rise to a plateau value for $-\log [H^+] > 4$. The same was true for log (Si/Fe) released vs. $-\log [H^+]$ (data not shown). Chorover and Sposito (1995b) also observed a plateau, near log (Si/Al) $\approx 0$, for $-\log [H^+] > 4$. Further insight as to this trend in Si/Al release is obtained by plotting the relative intensity of light scattering against log (Si/Al) for the supernatant solutions (Fig. 10). A very sharp maximum in the scattered light intensity near log (Si/Al) $\approx 0.5$ is seen for both soils irrespective of equilibration time. Plots of the data of Chorover and Sposito (1995b) made in this way also exhibited a sharp maximum, but at log (Si/Al) $\approx 0$ (data not shown). This light-scattering distribution indicates that the particles released into solution during our dissolution experiments have Si/Al molar ratios near 3 (and possibly near 1 in the experiments of Chorover and Sposito, 1995b). The rising portion of the graphs in Fig. 9 thus represents soluble released forms of Si and Al, while the plateau portion represents both soluble species and dispersed colloidal forms that are relatively enriched in Si.

The p.m.d. in Figs. 1–3 appears to lie between 3 and 4. The p.z.n.c. of the two soil samples is near 3.2 and that of specimen Georgia kaolinite is near 3.5 (Schroth and Sposito, 1997). The isoelectric point (i.e.p.) of kaolinite also is near 3 (Buchanan and Oppenheim, 1968; Braggs et al., 1994); that of quartz is 2–3 (Sposito, 1992); and that of the Manaus soil colloids is in the range 2.0–2.5 (Chorover and Sposito, 1995c). Thus the p.m.d., when observed, is near the p.z.n.c. of the soil, whose value is consistent with p.z.n.c. and i.e.p. data for both kaolinite and quartz.

At $-\log [H^+] >$ p.z.n.c., colloid dispersion begins to occur because of an increasingly negative surface charge

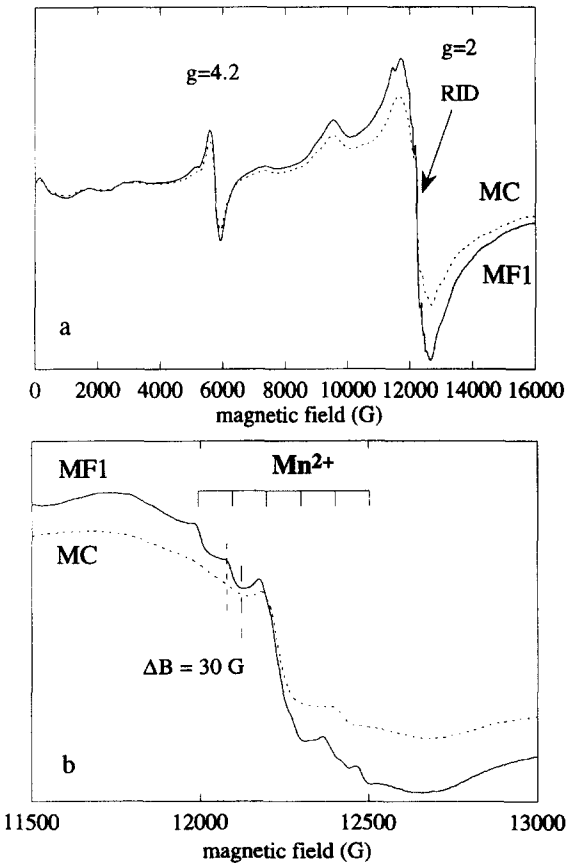


Fig. 8. (a) Q-band ESR spectra (laboratory temperature) of soils MC and MF1 before dissolution. (b) Narrow-range Q-band ESR spectra (laboratory temperature) of soils MF1 and MC before dissolution, showing Mn(II) features.

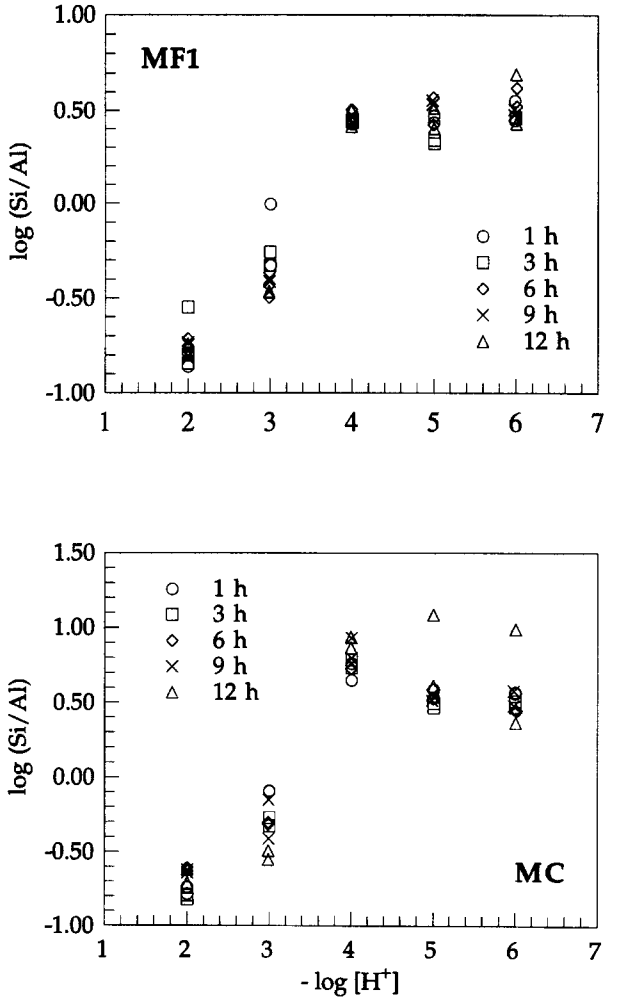


Fig. 9. Plot of log (Si/Al released) vs. initial $-\log [H^+]$ for all dissolution periods investigated.

buildup on kaolinite, quartz, and organic matter constituents. In soil sample MF1, the organic matter content is larger (but not the relative content of kaolinite or quartz, Table 1), the electrophoretic mobility of its colloids is more negative, and they flocculate at a substantially lower value of $-\log [H^+]$ than do the colloids in soil sample MC ($-\log [H^+] = 3.0$ for MF1 vs. 4.0 for MC (Chorover and Sposito, 1995c). Kretzschmar et al. (1997) have found the pH value at which Georgia kaolinite flocculates to drop from pH 4.6 in the presence of humic acid DOC at 1 mg $L^{-1}$ to pH < 3 when the humic acid DOC was increased to 4 mg $L^{-1}$. Thus, the absence of a clear p.m.d. for net Al and Fe release by sample MF1 at equilibration times >3 h is caused by the emergence of colloidal dispersion at a rather low $-\log [H^+]$ value $\approx 3$, which eventually masks the decline in soluble Al and Fe release with increasing $-\log [H^+]$, caused by metal readsorption on increasingly negative solid surfaces (Chorover and Sposito, 1995b).

### 4.2. Selective Dissolution of Quartz

X-ray diffraction (Fig. 5) and spectroscopic data (Figs. 6–8) indicated that kaolinite and iron oxides in the two soil samples were robust against short-term dissolution, even at $-\log [H^+] = 2$. The ESR spectra of both soil samples did not suggest changes in the Fe(III) or RID paramagnetic centers, and the homogeneous distribution of Fe(III), mainly in rhombically-disordered sites, also remained unchanged. These latter sites are thought to be at the boundaries of XRD-coherent domains (Gaite et al., 1993; Muller and Calas, 1993a) and connected to impurities that destroy the regularity of the kaolinite crystal (Herbillon, 1980; Mestdagh et al., 1980). The $Mn^{2+}$ signal in the ESR spectra did decrease slightly after dissolution, however. The six-line hyperfine structure (Fig. 8b) is similar to that reported by Muller and Calas (1993a) for kaolinitic tropical soils, which they assigned to $Mn^{2+}$ in occluded outer-sphere surface complexes on kaolinite. The observed decrease of this signal suggests that these surface complexes were slightly sensitive to dissolution.

The iron oxides in soils MF1 and MC are Al-substituted trace solid phases with variable structural order well known for iron oxide minerals in Brazilian Oxisols (Santos et al., 1989; Fontes and Weed, 1991). Electron microscope and XRD studies of kaolinite-iron oxide associations in Oxisols (Cambier and Prost, 1981; Boudeulle and Muller, 1988; Santos et al., 1989; Fontes, 1992) show the occurrence of iron oxides as both coatings and separate solid phases. The occur-

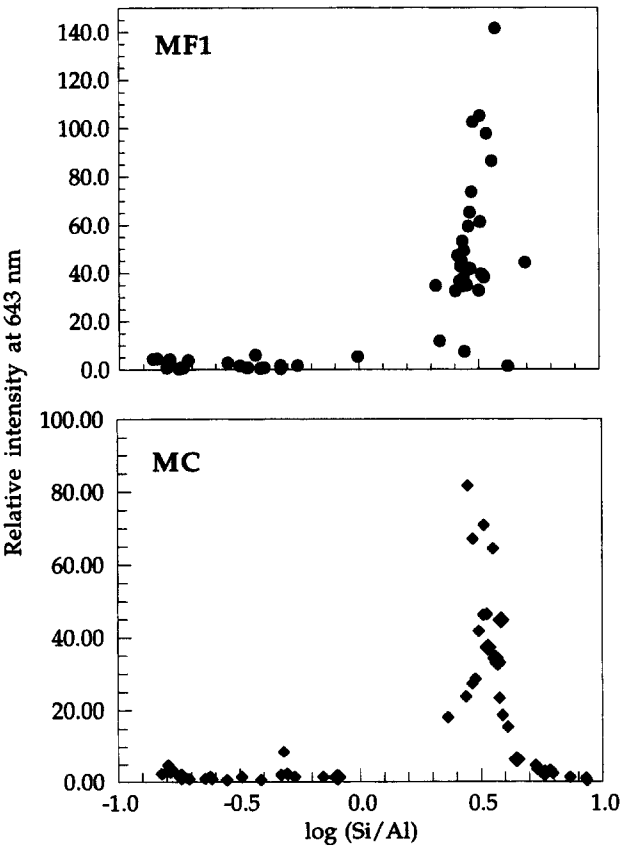


Fig. 10. Relative intensity of light scattered at 643 nm by supernatant solutions as a function of log (Si/Al) released for all dissolution periods investigated.

rence of organic matter as a separate solid phase also has been noted in these soils (Santos et al., 1989) and was strongly indicated in the present study by the merely uniform displacement of the diffuse reflectance spectra after chemical extraction of organic matter.

A significant loss of quartz during short-term dissolution was indicated by XRD data (Fig. 5 and Table 1). Highly-corroded quartz grains exhibiting coatings that are made up of iron, aluminum, and titanium oxides, as well as kaolinite, are a common feature in Oxisols (Eswaran and Stoops, 1979; Padmanabhan and Mermut, 1996). Herbillon (1980) has reviewed the considerable body of experimental evidence for quartz weathering of this type as the major source of soluble Si in Oxisols. Once in solution, Si can retard the weathering of kaolinite, especially if biocycling of the element by the vegetation canopy occurs (Herbillon, 1980; Lucas et al., 1993). Silica in solution also is known to retard the dissolution of aluminum and iron oxides (Brunn Hansen et al., 1994). In our experiments, the Si concentration in the supernatant solutions was always greater than 2 mol $m^{-3}$, indicating metastable equilibrium with colloidal silica (Dove, 1995). Calculation of the quartz mass loss, based on Si concentrations in the supernatant solutions that correspond to the experimental conditions in Fig. 5, leads to estimates of about 8–9 wt% reduction for soils MF1 and MC, in reasonable agreement with the reductions calculated from the results of direct XRD measurement (Table 1).

## 5. CONCLUSIONS

The point of minimum dissolution (p.m.d.) observed by Chorover and Sposito (1995b) for the release of Al and Fe after 3 h dissolution was shown to be an artifact resulting from the superposition of two pH- and time-dependent physicochemical processes: metal solubilization/readsorption and colloidal dispersion. At $-\log [H^+] >$ p.z.n.c., siliceous colloids containing Al and Fe are gradually dispersed into the aqueous phase and can contribute to the total metal concentration as measured conventionally by ICPAES. A distinct p.m.d. occurs, for any period of dissolution <12 h, if the colloidal dispersion process becomes significant only at a pH value well above that at which significant metal readsorption begins (Fig. 1, soil MC). A p.m.d. will not appear (Fig. 1, soil MF1) if colloidal dispersion initiates at a pH value that is competitively close to that at which metal readsorption begins. Increasing organic matter content, as in soil MF1 relative to soil MC, favors this latter situation.

Kaolinite and iron oxides were found to be unaffected by the short time (<12h) dissolution process investigated. Evidence for iron oxides as both coatings and occlusions; for $Mn^{2+}$ as an occluded outer-sphere surface complex on kaolinite; and for organic matter as a separate solid phase (as opposed to being a mineral coating) was adduced from DRS and ESR spectra. Quartz, by contrast, was observed to dissolve significantly during 12 h of dissolution (Table 1 and Fig. 5), producing Si concentrations >2 mol $m^{-3}$ that are consistent with the formation of colloidal silica. This phenomenon, well known as a major feature of Oxisol weathering (Herbillon, 1980), can serve to preserve kaolinite in these soils when it is coupled to the natural biocycling of Si (Lucas et al., 1993).

*Acknowledgments*—The authors are much obliged to Cheryl Palm, Peter Motavalli, Paul Smithson, and Jon Chorover for providing the soil samples and physicochemical data on them. Facilities for making the XRD, DRS, and ESR measurements were provided by the Laboratoire de Minéralogie-Cristallographie (Universities of Paris VI and VII, France). We thank Gwenaelle Lauquet and Philippe Ildefonse for assistance in acquisition of X-ray diffractograms and ESR spectra, Paul Brooks for assistance with the ICPAES analyses, and Guillaume Morin for help in interpreting the XRD data. The manuscript was greatly improved by the critical and constructive comments of Kathryn L. Nagy, Carl S. Kirby, and two anonymous referees. Thanks to Angela Zabel for excellent preparation of the typescript.

*Editorial handling:* J. D. Rimstidt

## REFERENCES

Allard T., Malengreau N., and Muller J.-P. (1992) Approche spectroscopique de la typologie des kaolins des Charentes. Doc. Minist. Rech. Espace, Paris, 461–478.

Angel B. R., Jones J. P. E., and Hall P. L. (1974) Electron spin resonance of doped synthetic kaolinite. *Clays Clay Mineral.* **10,** 247–255.

Bailey S. W. (1980) Structures of layer silicates. In *Crystal Structures of Clay Minerals and Their X-ray Identification* (ed. G. W. Brindley and G. Brown), pp. 1–123. Mineral. Soc.

Barron V. and Torrent J. (1986) Use of the Kubelka-Munk theory to study the influence of iron oxides on soil colour. *J. Soil Sci.* **37,** 499–510.

Bish D. L. and Von Dreele R. B. (1989) Rietveld refinement of non-hydrogen atomic positions in kaolinite. *Clays Clay Mineral.* **37,** 289–296.

Boudeulle M. and Muller J.-P. (1988) Structural characteristics of hematite and goethite and their relationships with kaolinite in a laterite from Cameroon. A TEM study. *Bull. Minéral.* **111,** 149–166.

Braggs B., Fornasiero D., Ralston J., and St. Smart R. (1994) The effect of surface modification by an organosilane on the electrochemical properties of kaolinite. *Clays Clay Mineral.* **42,** 123–136.

Brindley W. G., Kao C. C., Harrison J. L., Lipsicas M., and Raythatha R. (1986) Relation between structural disorder and other characteristics of kaolinites and dickites. *Clays Clay Mineral.* **34,** 239–249.

Brunn Hansen H. C., Raben-Lange B., Raulund-Rasmussen K., and Borggaard O. K. (1994) Monosilicate adsorption by ferrihydrite and goethite at pH 3–6. *Soil Sci.* **158,** 40–46.

Buchanan A. S. and Oppenheim R. C. (1968) The surface chemistry of kaolinite. *Aust. J. Chem.* **21,** 2367–2371.

Cahill J. E. (1979) Derivative spectroscopy: Understanding its application. Amer. Lab., Vol. 11, 79–85.

Cambier P. and Prost R. (1981) Etude des associations argile-oxyde: Organisation des constituants d'un matériau ferallitique. *Agronomie* **1,** 713–722.

Chorover J. and Sposito G. (1995a) Surface charge characteristics of kaolinitic tropical soils. *Geochim. Cosmochim. Acta* **59,** 875–884.

Chorover J. and Sposito G. (1995b) Dissolution behavior of kaolinitic tropical soils. *Geochim. Cosmochim. Acta* **59,** 3109–3121.

Chorover J. and Sposito G. (1995c) Colloid chemistry of kaolinitic tropical soils. *Soil Sci. Soc. Amer. J.* **59,** 1558–1564.

Clozel B., Allard T., and Muller J.-P. (1994) Nature and stability of radiation-induced defects in natural kaolinites: New results and a reappraisal of published works. *Clays Clay Mineral.* **42,** 657–666.

Dove P. (1995) Kinetic and thermodynamic controls on silica reactivity in weathering environments. *Rev. Mineral.* **31,** 235–290.

Eswaran H. and Stoops G. (1979) Surface textures of quartz in tropical soils. *Soil Sci. Soc. Amer. J.* **43,** 420–424.

Farmer V. C., Russell J. D., and Smith B. F. L. (1983) Extraction of inorganic forms of translocated aluminum, iron, and silicon from a podzol Bs horizon. *J. Soil Sci.* **34,** 571–576.

Fontes M. P. F. (1992) Iron oxide-clay mineral association in Brazil-

ian oxisols: A magnetic separation study. *Clays Clay Mineral.* **40,** 175–179.

Fontes M. P. F. and Weed S. B. (1991) Iron oxides in selected Brazilian Oxisols: I. Mineralogy. *Soil Sci. Soc. Amer. J.* **55,** 1143–1149.

Gaite J.-M., Ermakoff P., and Muller J.-P. (1993) Characterization and origin of two $Fe^{3+}$ EPR spectra in kaolinite. *Phys. Chem. Mineral.* **20,** 242–247.

Hall P. L. (1980) The application of electron spin resonance spectroscopy to studies of clay minerals: I. Isomorphous substitutions and external surface properties. *Clays Clay Mineral.* **15,** 321–335.

Herbillon A. J. (1980) Mineralogy of oxisols and oxic materials. In *Soils with Variable Charge* (ed. B. K. Theng), pp. 109–126. New Zealand Soc. Soil Sci.

Hétier J. M. and Jeanroy E. (1973) Solubilisation différentielle du fer, de la silice et de l'aluminum part le réactif oxalate-dithionite et la soude diluée. *Pédol.* **23,** 85–89.

Hugenin R. L. and Jones J. L. (1986) Intelligent information extraction from reflectance spectra: Absorption band positions. *J. Geophys. Res.* **91,** 585–589, 598.

Karickhoff S. W. and Bailey G. W. (1973) Optical absorption spectra of clay minerals. *Clays Clay Mineral.* **21,** 59–70.

Kastner M. (1979) Silica polymorphs. *Rev. Mineral.* **6,** 99–109.

Kretzschmar R., Hesterberg D., and Sticher H. (1997) Effects of adsorbed humic acid on surface charge and flocculation of kaolinite. *Soil Sci. Soc. Amer. J.* **61,** 101–108.

Lucas Y., Luizão F. J., Chauvel A., Rouiller J., and Nahon D. (1993) The relation between biological activity in the rain forest and mineral composition of soils. *Science* **260,** 521–523.

Malengreau N., Muller J.-P., and Calas G. (1994) Iron-speciation in kaolins: A diffuse reflectance study. *Clays Clay Mineral.* **42,** 137–147.

Malengreau N., Muller J.-P., and Calas G. (1995) Spectroscopic approach for investigating the status and mobility of Ti in kaolinitic materials. *Clays Clay Mineral.* **43,** 615–621.

Malengreau N., Bedidi A., Muller J.-P., and Herbillon A. J. (1996) Spectroscopic control of iron oxide dissolution in two ferralitic soils. *Eur. J. Soil Sci.* **47,** 13–20.

Malengreau N., Weidler P. G., and Gehring A. U. (1997) Iron oxides in laterites: a combined mineralogical, magnetic, and diffuse reflectance study. *Schweiz. Mineral. Petrogr. Mitt.* **77,** 13–20.

Meads R. E. and Malden P. J. (1975) Electron spin resonance in natural kaolinites containing $Fe^{3+}$ and other transition metal ions. *Clays Clay Mineral.* **10,** 313–345.

Mehra O. P. and Jackson M. L. (1960) Iron oxide removal from soil and clays by a dithionite-citrate system buffered with sodium carbonate. *Clays Clay Mineral.* **7,** 317–327.

Mestdagh M. M., Vielvoye L., and Herbillon A. J. (1980) Iron in kaolinite: II. The relationship between kaolinite crystallinity and iron content. *Clays Clay Mineral.* **15,** 1–13.

Michalopoulos P. and Aller R. C. (1995) Rapid clay mineral formation in Amazon delta sediments: Reverse weathering and oceanic elemental cycles. *Science* **270,** 614–617.

Morin G. (1994) Cristallochimie du fer dans les bauxites. Application à l'étude du gisement de Bidi-Koum (Guinée). Ph.D. dissertation, Univ. Paris VII.

Motavalli P. P., Palm C. A., Elliott E. T., Parton W. J., and Frey S. D. (1994) A comparison of laboratory modeling simulation methods for estimating soil carbon pools in tropical soils. *Soil Biol. Biochem.* **26,** 935–944.

Motavalli P. P., Palm C. A., Elliott E. T., Parton W. J., Frey S. D., and Smithson P. C. (1995) Nitrogen mineralization in humid tropical forest soils: Mineralogy, texture, and measured nitrogen fractions. *Soil Sci. Soc. Amer. J.* **59,** 1168–1175.

Mulder J. and Stein A. (1994) The solubility of aluminum in acidic forest soils. *Geochim. Cosmochim. Acta* **58,** 85–94.

Muller J.-P. and Calas G. (1993a) $Mn^{2+}$ bearing kaolinites from lateritic weathering profiles: Geochemical significance. *Geochim. Cosmochim. Acta* **57,** 1029–1034.

Muller J.-P. and Calas G. (1993b) Genetic significance of paramagnetic centers in kaolinite. In *Kaolin Genesis and Utilization* (ed. H. H. Murray et al.), pp. 261–289. Clay Minerals Soc.

Padmanabhan E. and Mermut A. R. (1996) Submicroscopic structure of iron coatings on quartz grains in tropical environments. *Clays Clay Mineral.* **44,** 801–810.

Post J. E. and Bish D. L. (1988) Rietveld refinement of the todorokite structure. *Amer. Mineral.* **73,** 861–869.

Reinsch C. H. (1967) Smoothing by spline functions. *Numerische Mathe.* **10,** 177–183.

Santos M. C. D., Mermut A. R., and Ribeiro M. R. (1989) Submicroscopy of clay micro aggregates in an oxisol from Pernambuco, Brazil. *Soil Sci. Soc. Amer. J.* **53,** 1895–1901.

Schroth B. and Sposito G. (1997) Surface charge properties of kaolinite. *Clays Clay Miner.* **45,** 85–91.

Schwertmann U. (1985) The effect of pedogenic environments on iron oxide minerals. *Adv. Soil Sci.* **1,** 171–200.

Schwertmann U. and Herbillon A. J. (1992) Some aspects of fertility associated with the mineralogy of highly weathered tropical soils. In *Myths and Science of Soils of the Tropics* (ed. R. Lal and P. A. Sánchez); *Soil Sci. Soc. Amer. Spec. Publ.* **29,** 47–59.

Singh R. and Gilkes R. J. (1993) Properties of soil kaolinites from southwestern Australia. *J. Soil Sci.* **43,** 645–667.

Sposito G. (1992) Characterization of particle surface charge. In *Environmental Particles* (ed. J. Buffle and H. P. van Leeuwen), Vol. 1, pp. 291–314. Lewis Publ.

Stevenson F. J. (1994) *Humus Chemistry.* Wiley.

Tamm O. (1922) Um best äwmning ow de oorganiska komponenterna i markens gelcomplex. *Medd. Statens Skogsförsökanst.* **19,** 385–404.

Weidner V. R. and Hsia J. J. (1981) Reflection properties of pressed polytetrafluoroethylene powder. *J. Opt. Soc. Amer.* **71,** 856–861.

Wendlandt W. W. M. and Hecht H. G. (1996) *Reflectance Spectroscopy.* Interscience.